An XFEM Model for Carbon Sequestration

Journal:	*International Journal for Numerical Methods in Engineering*
Manuscript ID:	NME-Feb-14-0085
Wiley - Manuscript type:	TB70
Date Submitted by the Author:	12-Feb-2014

Complete List of Authors:	Ladubec, Chris; University of Waterloo, Civil and Environmental Engineering Gracie, Robert; University of Waterloo, Civil and Environmental Engineering Craig, James; University of Waterloo, Civil and Environmental Engineering

Keywords:	Extended finite element method, Carbon Sequestration, Multiphase flow, XFEM, Multifield systems, Petrov-Galerkin

INTERNATIONAL JOURNAL FOR NUMERICAL METHODS IN ENGINEERING
Int. J. Numer. Meth. Engng 2014; **00**:1–17
Published online in Wiley InterScience (www.interscience.wiley.com). DOI: 10.1002/nme

An XFEM Model for Carbon Sequestration†

Chris Ladubec, Robert Gracie*, James Craig

Department of Civil and Environmental Engineering, University of Waterloo, 200 University Ave West, Waterloo, Ontario, Canada.

SUMMARY

A two-phase flow extended finite element method (XFEM) model is presented to analyze the injection and sequestration of carbon dioxide (CO_2) in deep saline aquifers. Carbon sequestration is a multiscale problem, involving length scales over four orders of magnitude–from injection well diameter scale to the aquifer scale. XFEM is introduced to accurately approximate near injection well pressure behaviour with elements significantly larger than the injection well diameter. We present a vertically averaged multiphase flow model that combines XFEM to approximate the pressure field, with a Streamline Upwind Petrov-Galerkin / Finite Element / Finite Difference method (SUPG-FEM-FDM) to approximate the distribution of CO_2 in the aquifer. Near well enrichment functions are presented along with the solution procedure for the coupled problem. Two examples are presented; in the first, CO_2 injection into a perfectly horizontal aquifer is model with both XFEM and FEM-based methods. It is shown that the XFEM provides improved accuracy in the prediction of pressure. The impact and selection of the stabilization coefficient of the SUPG-FEM-FDM is also discussed. In the second example, the XFEM and SUPG-FEM-FDM model are applied to a more realistic model of an inclined aquifer. Here the XFEM-based model is shown to correctly capture the buoyancy driven migration of CO_2 in a deep saline aquifer. Copyright © 2014 John Wiley & Sons, Ltd.

Received . . .

KEY WORDS: Multiphase Flow; Carbon Sequestration; eXtended Finite Element Method; XFEM LaTeX 2_ε; *Int. J. Numer. Meth. Engng*

1. INTRODUCTION

Carbon sequestration is an operation where carbon dioxide (CO_2) from point source emitters, such as coal-fired power plants, is injected into deep geological structures for long term storage. Ideal storage locations are deep saline aquifers that have an impermeable caprock above to prevent the CO_2 from leaking into overlaying aquifers.

Deep saline aquifers are composed of porous rock such as sandstone and initially contain brine (salt water). The resident brine is displaced when the CO_2 is injected. At the depths of these aquifers the temperatures and pressures are such that the CO_2 exists in a supercritical state. The supercritical CO_2 is less dense than the host brine, and thus there will be a buoyancy drive causing the CO_2 to rise and float on top of the brine.

Carbon sequestration is a multiscale problem. There is a large difference in the timescales of relevant processes and there are large differences in spatial scales. The horizontal dimensions of the aquifers are measured in kilometers, but the diameter of the injection wells is measured in centimeters. To accurately resolve the pressure field in the vicinity of an injection or abandoned wells using traditional numerical methods would require a prohibitively fine discretization near the wells.

*Correspondence to: Dr. Robert Gracie at rgracie@uwaterloo.ca
†In honour of Professor Ted Belytschko

In this paper, an eXtended Finite Element Method (XFEM) method for accurate and efficient modeling of the pressure field resulting from injecting CO_2 into a deep saline aquifer using a vertically averaged multiphase flow formulation is presented. XFEM is then coupled to a Streamline Upwind Petrov-Galerkin/ Finite Element Method/Finite Difference Method (SUPG-FEM-FDM) to model the evolution of the average saturation of each phase in the aquifer. This article follows earlier works by the authors on XFEM-based single phase aquifer flow models [1, 2].

The XFEM was comprehensively developed by Belytschko and co-workers over the past 15 years [3, 4, 5, 6] . It was first applied to the simulation of the singularities and discontinuities found in linear elastic fracture mechanics [7, 8]. Later applications focussed on dynamic crack propagation [9, 10, 11], multiscale analysis [12, 13, 14], and material modelling [15, 16, 17].

Comparably less attention has been given to the application of XFEM to multiphase flow. Some notable exceptions are the two-dimensional two-phase flow works of Chessa and Belytschko [18] and Cheng and Fries [19], the three-dimensional two-phase flow models of Sauerland and Fries [20] and the analysis of partially saturated porous media of Mohammadnejad and Khoei [21]. One of the major differences between these earlier works and that present here, is that they focus on two and three dimensional models, whereas, the present model is quasi-three dimensional, leading to different governing equations, different representation of the interface between fluid phases, and different enrichment functions. Furthermore, the focus here is on the singular behaviour near wells.

This article is organized as follows. We present the equations governing conservation of mass in the vertically averaged multiphase flow of CO_2 and brine in a porous medium in Section 2. In Section 3, 4 and 5, the government equations, weak form, and discrete equations, respectively. Two numerical examples that demonstrate the capabilities of the outlined model are presented is Section 6 and conclusions are given in Section 7.

2. PROBLEM STATEMENT

Consider a saline aquifer, bounded from above and below by impermeable aquicludes, as illustrated in the cross-section shown in Figure 1. CO_2 is injected into the saline aquifer displacing the host brine fluid. Since the density of the CO_2 is less than the brine it floats on top of the brine and spreads laterally. The injection well acts as a point source, with a locally singular pressure field. Singlular pressure fields are also found near hydraulic connections between adjacent aquifers, such as in the vicinity of abandoned wells, faults and fractures [1]. In this paper, we present a computationally efficient methodology to model the injection of CO_2 into a carbon sequestration system. Vertically averaged mass balance equations [22] are used to describe the pressure distribution and the average saturation distribution of CO_2 in the injection aquifer.

The use of a vertically averaged formulation allows us to reduce the dimensionality of the problem from three to two by integrating the governing equations over the depth of the aquifers [23, 24, 25, 26]. Vertical averaging thus reduces the number of degrees of freedom in the system by one third, thus increasing the computational efficiency of the resulting numerical model. Reducing the dimensionality of the problem is generally considered a reasonable approximation since the depth of the aquifers is quite small compared to the horizontal dimensions of the aquifer [22].

The governing equations adopted in this paper assume:

- Chemical, thermal and mechanical effects are negligible;
- The brine, CO_2 and solid matrix are incompressible;
- The viscosity and density of brine and CO_2 are constant;
- The interface between the brine and CO_2 is sharp and the capillary pressure is zero;
- The pressure in the aquifer varies hydrostatically through the depth of the aquifer.

The governing equations are the mass balance equations for brine and CO_2 which are combined with two equations describing vertically averaged fluxes of each phase using a multiphase extension of Darcy's law [22].

DOI: 10.1002/nme

The mass balance equations for the CO_2 and brine phases in the aquifer are:

$$\phi(1 - S_{res,B})\frac{\partial h}{\partial t} + \nabla \cdot \hat{\mathbf{q}}_C = q_{C,inj} \tag{1}$$

$$\phi(1 - S_{res,B})\frac{\partial (H - h)}{\partial t} + \nabla \cdot \hat{\mathbf{q}}_B = 0 \tag{2}$$

where ϕ is the porosity of the aquifer, $S_{res,B}$ is residual saturation of the brine, $h(\mathbf{x}, t)$ is the depth of the CO_2, $\hat{\mathbf{q}}_C(\mathbf{x}, t)$ is the vertically averaged CO_2 flux, $\hat{\mathbf{q}}_B(\mathbf{x}, t)$ is the vertically averaged brine flux, $q_{C,inj}(\mathbf{x}, t)$is the source term to account for the injection of CO_2 into the aquifer.

CO_2 is assumed to be injected from a point source and is defined as:

$$q_{C,inj} = Q_{inj}\delta(\mathbf{x} - \mathbf{x_{inj}}) \tag{3}$$

where Q_{inj} is the injection rate (e.g. m^3/d), and $\delta()$ is the Dirac delta function.

The vertically averaged fluxes are given by the multiphase extension of Darcy's Law [22]:

$$\hat{\mathbf{q}}_C = -h\frac{\mathbf{k}k_{rel,C}}{\mu_C}(\nabla p_{bot} - \rho_B g \nabla H + \Delta\rho g \nabla h + \rho_C g \nabla z_{top}) \tag{4}$$

$$\hat{\mathbf{q}}_B = -(H - h)\frac{\mathbf{k}}{\mu_B}(\nabla p_{bot} + \rho_B g \nabla z_{bot}) \tag{5}$$

where $\mathbf{k}$ is the intrinsic permeability of the aquifer, $k_{rel,C}$ is the relative permeability, μ_C is the viscosity of CO_2, μ_B is the viscosity of brine, $p_{bot}(\mathbf{x}, t)$ is the pressure at the bottom of the aquifer, ρ_C is the density of CO_2, ρ_B is the density of the brine, $\Delta\rho = \rho_B - \rho_C$, g is the gravitational constant, $z_{top}(\mathbf{x})$ is the vertical depth of the top of the aquifer, $z_{bot}(\mathbf{x})$ is the vertical depth of the bottom of the aquifer, and $H(\mathbf{x})$ is the thickness of the aquifer.

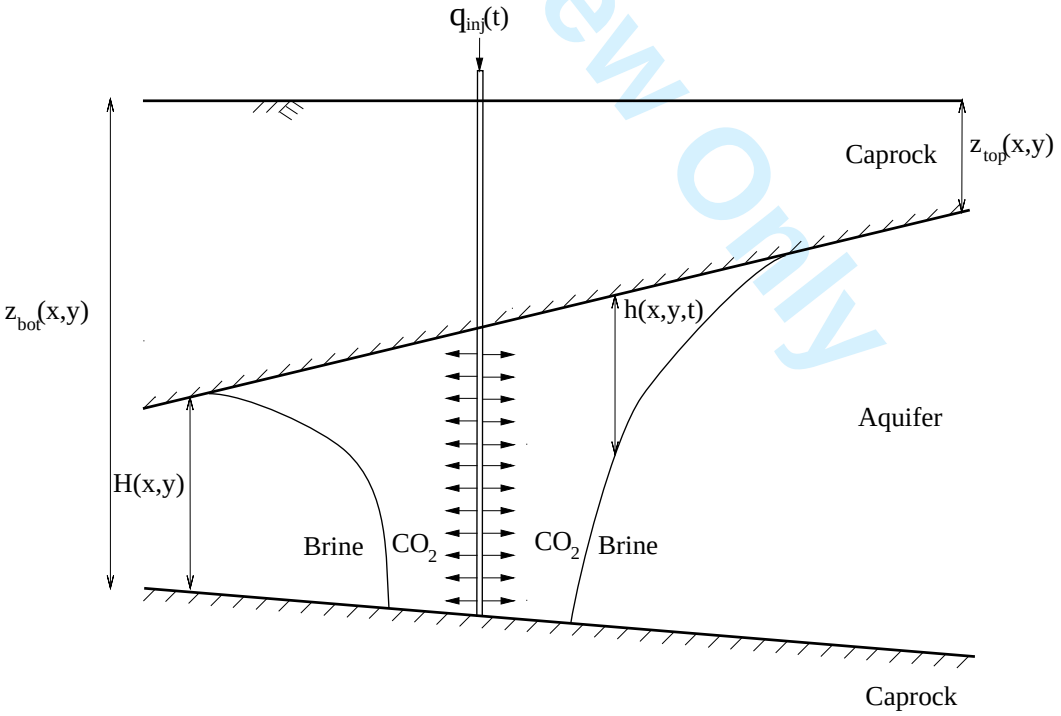

Figure 1. Defining parameters of carbon sequestration model.

DOI: 10.1002/nme

3. STRONG FORM

The solution approach we take is to manipulate (1) and (2) to arrive at two equations: one that is solved for pressure (pressure equation) and the second that is solved for the average saturation distribution (saturation equation).

We first obtain the strong form of the pressure equation and saturation equation from (1) and (2) combined with (4) and (5). The pressure equation is obtained by adding the mass balance equations for each phase. The transient term disappears and the pressure equation becomes an elliptical steady state equation, i.e., a Poisson-type equation. This leads to an instantaneous propagation of changes in pressure through the domain Ω. The strong form of the pressure equation is: Find $p_{bot}(\mathbf{x})$ such that:

$$\begin{aligned}&\nabla\cdot\left(h\frac{\mathbf{k}k_{REL}^{C}}{\mu_C}(\nabla p_{bot}+\Delta\rho g\nabla h-\rho_B g\nabla H+\rho_C g\nabla z_{top})\right)\\&+\nabla\cdot\left((H-h)\frac{\mathbf{k}}{\mu_B}(\nabla p_{bot}+\rho_B g\nabla z_{bot})\right)\\&=q_{inj,C},\mathbf{x}\in\Omega\end{aligned}\tag{6}$$

and

$$p_{bot}(\mathbf{x},t)=\overline{p}_{bot}(\mathbf{x},t)\text{ on }\Gamma_p\tag{7}$$
$$\hat{\mathbf{q}}_C(\mathbf{x},t)=\overline{\mathbf{q}}_C(\mathbf{x},t)\text{ on }\Gamma_q\tag{8}$$
$$\hat{\mathbf{q}}_B(\mathbf{x},t)=\overline{\mathbf{q}}_B(\mathbf{x},t)\text{ on }\Gamma_q\tag{9}$$

where $\Gamma_p\cup\Gamma_q$ is the boundary of Ω and $\Gamma_p\cap\Gamma_q=\emptyset$.

The saturation equation is obtained directly from the mass balance equation for the brine, (2) and (5). The strong form of the saturation equation is: Find $h(\mathbf{x},t)$ such that:

$$\begin{aligned}&\phi(1-S_{res,B})\frac{\partial(H-h)}{\partial t}-\nabla\cdot\left((H-h)\frac{\mathbf{k}}{\mu_B}(\nabla p_{bot}+\rho_B g\nabla z_{bot})\right)\\&=0,\mathbf{x}\in\Omega,\mathrm{t}\in[0,t_{end}]\end{aligned}\tag{10}$$

$$h(\mathbf{x},t)=\overline{h}(\mathbf{x},t)\text{ on }\Gamma_h\tag{11}$$
$$h(\mathbf{x},0)=h_o(\mathbf{x})\text{ on }\Omega\tag{12}$$

where Γ_h is the boundary of Ω.

4. WEAK FORM

In this section, the weak forms of the pressure equation and the saturation equation are presented. The weak form of the pressure equation for the pressure at the bottom of the aquifer (6) is: find

DOI: 10.1002/nme

$p_{bot}(\mathbf{x}) \in W$ such that

$$\begin{aligned}
&\int_\Omega (\nabla w)^T (H-h)\frac{\mathbf{k}}{\mu_B}\nabla p_{bot} d\Omega + \int_\Omega (\nabla w)^T (H-h)\frac{\mathbf{k}}{\mu_B}\rho_B g \nabla z_{bot} d\Omega \\
&+ \int_\Omega (\nabla w)^T h \frac{\mathbf{k}k_{rel,C}}{\mu_C}\Delta\rho g \nabla h d\Omega - \int_\Omega (\nabla w)^T h \frac{\mathbf{k}k_{rel,C}}{\mu_C}\rho_B g \nabla H d\Omega \\
&+ \int_\Omega (\nabla w)^T h \frac{\mathbf{k}k_{rel,C}}{\mu_C}\rho_C g \nabla z_{top} d\Omega - \oint_\Gamma w^T \hat{\mathbf{q}}_{\mathbf{B}}^T \mathbf{n} d\Gamma \\
&+ \int_\Omega (\nabla w)^T h \frac{\mathbf{k}k_{rel,C}}{\mu_C}\nabla p_{bot} d\Omega - \oint_\Gamma w^T \hat{\mathbf{q}}_{\mathbf{C}}^T \mathbf{n} d\Gamma \\
&= \int_\Omega w^T q_{inj,C} d\Omega, \forall w \in W_0.
\end{aligned} \tag{13}$$

The function spaces are given as

$$\begin{aligned}
W &= \{p_{bot}(\mathbf{x}) | p_{bot}(\mathbf{x}) \in H^1, p_{bot}(\mathbf{x}) = \overline{p}_{bot} \text{ on } \Gamma_p\} \\
W_0 &= \{w(\mathbf{x}) | w(\mathbf{x}) \in H^1, w(\mathbf{x}) = 0 \text{ on } \Gamma_p\}
\end{aligned} \tag{14}$$

The weak form of the saturation equation is: find $h(\mathbf{x},t) \in U$ such that

$$\begin{aligned}
&\int_\Omega v^T \phi (1 - S_{RES,B}) \frac{\partial (H-h)}{\partial t} d\Omega + \int_\Omega (\nabla v)^T (H-h)\frac{\mathbf{k}}{\mu_B}(\nabla p_{bot} + \rho_B g \nabla z_{bot}) d\Omega \\
&= \oint_\Gamma v^T \hat{\mathbf{q}}_B^T \mathbf{n} d\Gamma, \forall v \in U_0.
\end{aligned} \tag{15}$$

where U and U_0 are the appropriate function spaces for $h(\mathbf{x},t)$ and $v(\mathbf{x},t)$, respectivley.

5. DISCRETE EQUATIONS AND APPROXIMATION

In this section the discretization of the weak forms of the pressure and the saturation equation are presented. The pressure is discretized in space using the eXtended Finite Element Method (XFEM) and the CO_2 saturation is discretized using an Streamline Upwind Petrov-Galerkin Finite Element Method (SUPG-FEM) in space and a Finite Difference Method (FDM) in time.

5.1. XFEM Approximation of the Pressure Equation

The solution to the pressure equation (6) is known to be singular at the injection well. To better approximate the pressure field, an XFEM approximation is adopted. The key to the XFEM is that the FEM approximation is enriched in the vicinity of the injection wells with functions that capture the asymptotic behaviour near the well. In contrast, an FEM model would require a fine mesh around the wells in order to obtain accurate solutions. As mentioned, XFEM was previously used to model single phase porous media flow in an aquifer [1, 2]. For the multiphase XFEM model present here, we investigate the use of the same enrichment function.

The enrichment function for the pressure near well α is

$$\phi_\alpha(\mathbf{x}) = \begin{cases} \log(r_\alpha(\mathbf{x})), r_\alpha > r_w \\ \log(r_w), r_\alpha \leq r_w \end{cases} \tag{16}$$

where r_α is distance to the center of the well number,α, and r_w is the radius of the well.

$$r_\alpha(\mathbf{x}) = ||\mathbf{x} - \mathbf{x}_\alpha^{inj}|| \tag{17}$$

where $\mathbf{x}_\alpha^{inj}$ are the spatial coordinates of the injection wells.

DOI: 10.1002/nme

The XFEM approximation of pressure is given by

$$p(\mathbf{x}) = \sum_{I \in \mathcal{N}} N_I(\mathbf{x}) p_I + \sum_{\alpha=1}^{n_{inj}} w_\alpha(\mathbf{x}) \phi_\alpha(\mathbf{x}) \sum_{J \in S_\alpha} N_J(\mathbf{x}) a_{\alpha J}, \mathbf{x} \in \Omega \tag{18}$$

where $\mathcal{N}$ is the set of all nodes, p_I is the pressure at node I, n_{inj} is the number of injection wells, S_α is the set of nodes in the enriched domain of well α (see Figure 2), $w_\alpha(\mathbf{x})$ is a weighting function that blends the enriched and unenriched parts of the domain ([27], [1]), $a_{\alpha J}$ are the enriched degrees of freedom, and $N_I(\mathbf{x})$ are the standard finite element basis functions.

The pressure approximation can be written in matrix form as:

$$p(\mathbf{x}) = \mathbf{N}\mathbf{p_{bot}} + \overline{\mathbf{N}}\mathbf{a} \tag{19}$$

where $\mathbf{N}$ is the matrix of standard FEM shape functions and $\overline{\mathbf{N}}$ is the matrix of the enriched shape functions. $\mathbf{p_{bot}}$ and $\mathbf{a}$ are vectors containing the standard FEM pressure degrees of freedom and the enriched degrees of freedom respectively.

$$\mathbf{p_{bot}}^T = \{p_1, p_2, ..., p_{nn}\} \tag{20}$$

$$\mathbf{a}^T = \{a_1, a_2, ..., a_{mm}\} \tag{21}$$

where nn and mm are the number of nodes in the mesh and the number of enriched nodes, respectively.

The blending weight function is define as

$$w(\mathbf{x}) = \sum_{I \in \mathcal{N}} N_I(\mathbf{x}) w_I \tag{22}$$

where w_I is one for an enriched node within the enrichment radius, r_{enr}, and w_I is zero for an enriched node outside the enrichment radius.

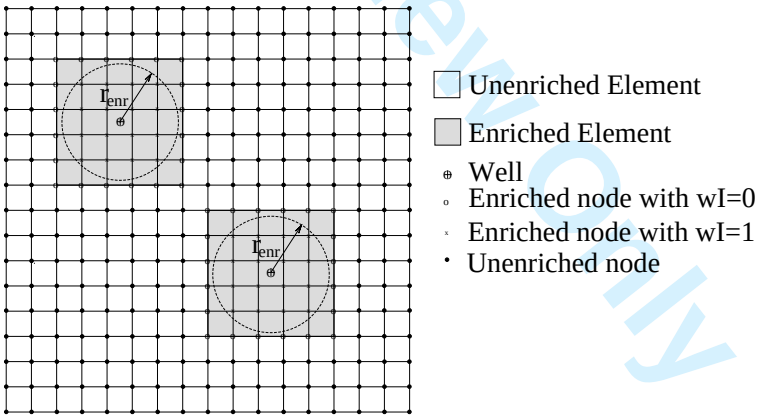

Figure 2. Enriched domain. $\mathcal{S}_\alpha$ is the set of nodes within the enrichment radius of well α

.

The XFEM discretization of the pressure equations are:

$$\mathbf{K}_{aquifer} \begin{Bmatrix} \mathbf{p_{bot}} \\ \mathbf{u} \end{Bmatrix} = \begin{Bmatrix} \mathbf{F_p} \\ \overline{\mathbf{F}}_\mathbf{p} \end{Bmatrix} \tag{23}$$

$$\mathbf{F_p} = \mathbf{F_{p1}} + \mathbf{F_{p2}} + \mathbf{F_{p3}} + \mathbf{F_{p4}} \tag{24}$$

$$\overline{\mathbf{F}}_\mathbf{p} = \overline{\mathbf{F}}_{\mathbf{p1}} + \overline{\mathbf{F}}_{\mathbf{p2}} + \overline{\mathbf{F}}_{\mathbf{p3}} + \overline{\mathbf{F}}_{\mathbf{p4}} \tag{25}$$

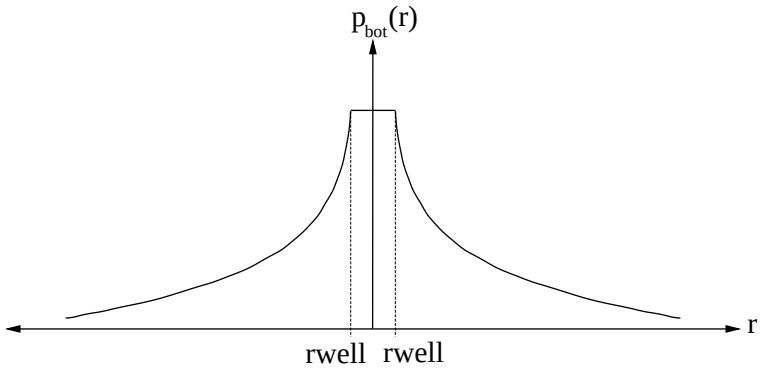

Figure 3. Illustration of the enrichment function.

$$\mathbf{K}_{aquifer} = \begin{bmatrix} \mathbf{K} & \overline{\mathbf{K}} \\ \overline{\mathbf{K}}^T & \overline{\overline{\mathbf{K}}} \end{bmatrix} \tag{26}$$

where $\mathbf{K_p}$ is the stiffness matrix, $\mathbf{F_{p1}}$ is the injection vector, $\mathbf{F_{p2}}$ is the boundary flux vector, $\mathbf{F_{p3}}$ is the buoyancy vector, and $\mathbf{F_{p4}}$ is the aquifer slope vector. $\overline{\mathbf{K}}_\mathbf{p}$ and $\overline{\overline{\mathbf{K}}}_\mathbf{p}$ are enriched stiffness matrices, $\overline{\mathbf{F}}_\mathbf{p1}$ is the enriched injection vector, $\overline{\mathbf{F}}_\mathbf{p2}$ is the enriched boundary flux vector, $\overline{\mathbf{F}}_\mathbf{p3}$ is the enriched buoyancy vector, and $\overline{\mathbf{F}}_\mathbf{p4}$ is the enriched aquifer slope vector.

The matrices and vectors are

$$K_{p,IJ} = \int_\Omega \mathbf{B}_I^\mathsf{T} \left(\frac{hk_{REL,C}}{\mu_C} + \frac{H-h}{\mu_B} \right) \mathbf{k}\mathbf{B}_J d\Omega, \forall I, J \in \mathcal{N} \tag{27}$$

$$\overline{K}_{p,IJ} = \int_\Omega \overline{\mathbf{B}}_I^\mathsf{T} \left(\frac{hk_{REL,C}}{\mu_C} + \frac{H-h}{\mu_B} \right) \mathbf{k}\mathbf{B}_J d\Omega, \forall I \in \mathcal{N}, \forall J \in \mathcal{S}_\alpha \tag{28}$$

$$\overline{\overline{K}}_{p,IJ} = \int_\Omega \overline{\mathbf{B}}_I^\mathsf{T} \left(\frac{hk_{REL,C}}{\mu_C} + \frac{H-h}{\mu_B} \right) \mathbf{k}\overline{\mathbf{B}}_J d\Omega, \forall I \in S_\alpha, \forall J \in \mathcal{S}_\beta \tag{29}$$

$$F_{p1,I} = \int_\Omega \mathbf{N}_I^\mathsf{T} q_{C,inj} d\Omega, \forall I \in \mathcal{N} \tag{30}$$

$$\overline{F}_{p1,I} = \int_\Omega \overline{\mathbf{N}}_I^\mathsf{T} q_{C,inj} d\Omega, \forall I \in \mathcal{S}_\alpha \tag{31}$$

$$F_{p2,I} = -\oint_\Gamma \mathbf{N}_I^\mathsf{T} (\overline{q}^B + \overline{q}^C) \mathbf{n} d\Gamma, \forall I \in \mathcal{N} \tag{32}$$

$$\overline{F}_{p2,I} = -\oint_\Gamma \overline{\mathbf{N}}_I^\mathsf{T} (\overline{q}^B + \overline{q}^C) \mathbf{n} d\Gamma, \forall I \in \mathcal{S}_\alpha \tag{33}$$

$$F_{p3,I} = -\int_\Omega \mathbf{B}_I^\mathsf{T} \frac{\mathbf{k}k_{rel,C}}{\mu_C} \Delta\rho g h \nabla h d\Omega, \forall I \in \mathcal{N} \tag{34}$$

$$\overline{F}_{p3,I} = -\int_\Omega \overline{\mathbf{B}}_I^\mathsf{T} \frac{\mathbf{k}k_{rel,C}}{\mu_C} \Delta\rho g h \nabla h d\Omega, \forall I \in \mathcal{S}_\alpha \tag{35}$$

$$F_{p4,I} = \int_\Omega \mathbf{B}_I^\mathsf{T} (h \frac{\mathbf{k}k_{rel,C}}{\mu_C} (\rho_B g \nabla H - \rho_C g \nabla z_{top}) - (H-h) \frac{\mathbf{k}}{\mu_B} \rho_B g \nabla z_{bot}) d\Omega, \forall I \in \mathcal{N} \tag{36}$$

$$\overline{F}_{p4,I} = \int_\Omega \overline{\mathbf{B}}_I^\mathsf{T} (h \frac{\mathbf{k}k_{rel,C}}{\mu_C} (\rho_B g \nabla H - \rho_C g \nabla z_{top}) - (H-h) \frac{\mathbf{k}}{\mu_B} \rho_B g \nabla z_{bot}) d\Omega, \forall I \in \mathcal{S}_\alpha \tag{37}$$

DOI: 10.1002/nme

where $\mathbf{B}$ and $\overline{\mathbf{B}}$ are matrices of the derivatives of the standard and enriched shape functions, respectively.

5.1.1. Numerical Integration Numerical integration of the unenriched elements in the pressure equation is performed using 2x2 Gauss quadrature. Enriched elements that do not contain a well are integrated using 4x4 Gauss quadrature. Enriched elements containing wells are integrated using an iterative bisection scheme as described in [1]. The subcells are then integrated using 3x3 Gauss quadrature if they are located outside the well radius, and using 1x1 Gauss quadrature if they are located within the well radius.

5.2. Stabilized Galerkin FEM - CN discretization of the Saturation Equation

An SUPG-FEM-FDM approximation is used to discretize the saturation equation. Space is discretized using an SUPG-FEM approach. SUPG is implemented as an added artificial diffusion term that counteracts the negative diffusion that occurs due to the Galerkin FEM discretization of the hyperbolic saturation equation (i.e., the advection equation). A Crank-Nicolson (trapezoidal) finite difference method is used to discretize the time domain.

The average saturation of the brine is approximated in space by:

$$h(\mathbf{x}) = \sum_{I \in \mathcal{N}} N_I(\mathbf{x}) h_I \tag{38}$$

The semi-discrete FEM saturation equations are given by:

$$[\mathbf{C_s}]\{\dot{\mathbf{h}}_\mathbf{B}\} + [\mathbf{K_s}]\{\mathbf{h_B}\} = \{\mathbf{F_s}\} \tag{39}$$

$$\mathbf{C}_s = \int_\Omega \mathbf{N^e}^T \phi(1 - S_{RES,B}) \mathbf{N^e} d\Omega \tag{40}$$

$$\mathbf{K}_{adv} = \int_\Omega \mathbf{B^e}^T \frac{\mathbf{k}}{\mu_B} (\nabla p_{bot} + \rho_B g \nabla z_{bot}) \mathbf{N^e} d\Omega \tag{41}$$

$$\mathbf{F}_s = \oint_\Gamma \mathbf{N^e}^T \overline{q}_B \mathbf{n} d\Gamma \tag{42}$$

where $\{\mathbf{h_B}\}$ is the unknown vector of brine depth in the aquifer and $h_B(\mathbf{x}, t) = H(\mathbf{x}) - h(\mathbf{x}, t)$, $\mathbf{C}_s$ is the mass matrix, $\mathbf{K}_{adv}$ is the advection matrix , $\mathbf{F}_s$ is the boundary flux vector. $\mathbf{N^e}$ are the shape functions for each element and $\mathbf{B^e}$ are the derivatives of the shape functions. The XFEM pressure approximation is utilized in the advection matrix, $\mathbf{K}_{adv}$ above. The Streamline Upwind Petrov-Galerkin (SUPG) method is used to stabilize the saturation equation, which is similar to a pure advection equation. SUPG is implemented using artificial diffusion as described in [28]. Artificial diffusion acts to offset the negative diffusion that is created due to the Galerkin FEM approach. The artificial diffusion to the system, which for the pure advection case simplifies to

$$\mathbf{K}_{SUPG} = \int_{\Omega^e} \mathbf{B^e}^T \tau \frac{H}{\phi(1 - S_{res,B})} \frac{\mathbf{k}}{\mu_B} |\nabla p_{bot} + \rho_B g \nabla z_{bot}| \mathbf{B^e d\Omega^e} \tag{43}$$

where τ is a parameter to control the amount of diffusion applied.

In the saturation equation, time is discretized using the finite difference method. This can be written as

$$\begin{aligned} &([\mathbf{C_s}] + \Delta t \theta [\mathbf{K_s}]^{n+1})\{\mathbf{h_B}\}^{n+1} = \\ &(([\mathbf{C_s}] - \Delta t(1-\theta)[\mathbf{K_s}]^n)\{\mathbf{h_B}\}^n + \Delta t(\theta\{\mathbf{F_s}\}^{n+1} + (1-\theta)\{\mathbf{F_s}\}^n)) \end{aligned} \tag{44}$$

where $[\mathbf{K_s}] = [\mathbf{K}_{adv}] + [\mathbf{K}_{SUPG}]$

In the above equation, $\theta = 0.5$ gives the Crank-Nicolson (CN) method. CN is an implicit scheme that is unconditionally stable and second order accurate (i.e. $O(h_e^2)$).

DOI: 10.1002/nme

5.3. Solution Procedure

The system of equations that we obtain from the discretization of the pressure and saturation equations are strongly coupled. A sequential solution strategy similar to IMPES (IMplicit Pressure Explicit Saturation) [29], which is common in the reservoir simulation community is adopted. In this solution scheme initial conditions for the saturation are specified and the initial pressure distribution is computed. Then for each timestep the saturation equation is solved using the pressure distribution from the previous timestep. The pressure distribution is then updated using the saturation distribution from the current timestep. This solution strategy is shown in Figure 4.

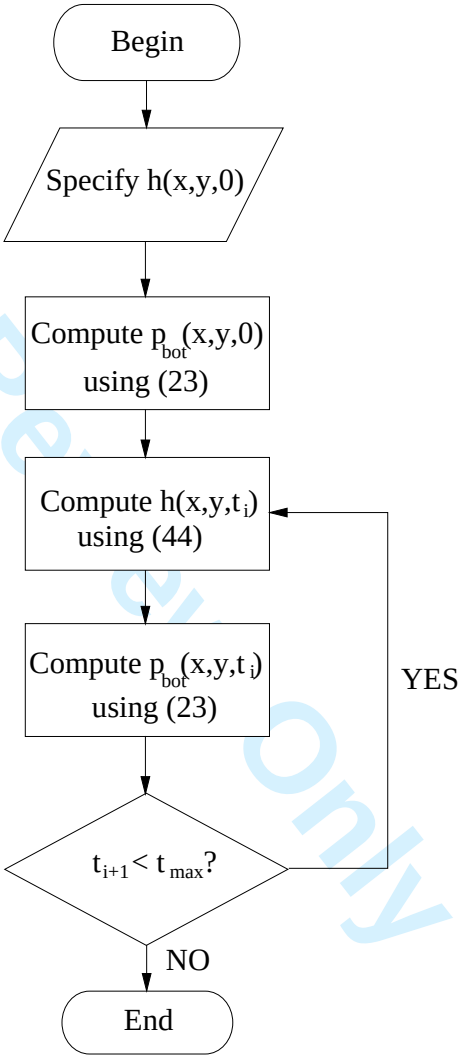

Figure 4. Solution strategy. Pressure is solved using (23) and saturation is solved using (44).

6. NUMERICAL EXAMPLES

The solution approach described in this paper is demonstrated using two examples.

DOI: 10.1002/nme

Table I. System properties for example 1.

Property	Value	Units
μ_B	5.11e-4	Ns/m^2
μ_C	6.11e-5	Ns/m^2
ρ_B	1099	kg/m^3
ρ_C	400	kg/m^3
$S_{res,B}$	0	-
ϕ	0.15	-
k_x	1e-15	m^2
k_y	1e-15	m^2
$k_{rel,C}$	1	-
q_{inj}	1600	m^3/d
r_w	0.15	m

6.1. *Example 1*

In this example CO_2 is injected into a brine filled aquifer. The setup of this problem is shown in Figure 5. The system properties are given in Table I. The aquifer is bounded above and below by impermeable caprock layers (aquicludes). Initially, the aquifer is filled with brine. The water table begins at the top boundary of the aquifer. CO_2 is injected at a constant rate of 1600 m^3/d. As the injection progresses, the CO_2 plume spreads throughout the aquifer.

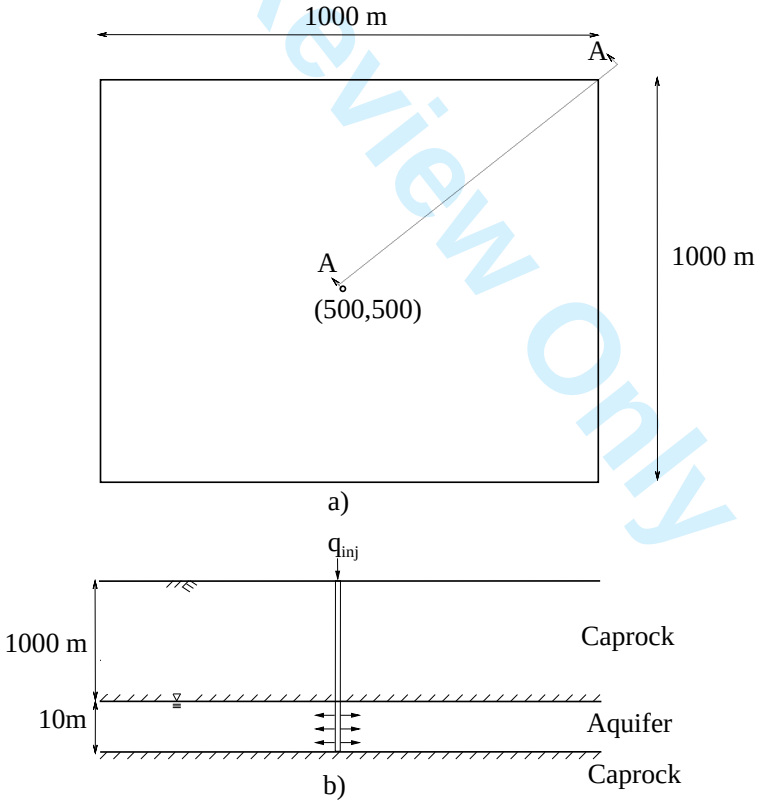

Figure 5. Set up of Example 1

Dirichlet boundary conditions of hydrostatic pressure are applied for the pressure equation along the whole boundary of the domain. An initial condition of $h(\mathbf{x}, 0) = 0$ throughout the domain is used (i.e. brine only). Dirichlet boundary conditions of $h(\mathbf{x}, t) = 0$ are imposed at all boundaries,

and as such the domain must be large enough so that the CO_2 plume remains far enough away from the domain boundaries. The simulation is conducted for a time of 3 days.

Figure 6 compares the pressures distributions for two XFEM and two FEM simulations with different mesh densities. The pressure is plotted along section A-A, as shown in Figure 5. It is clear that the XFEM simulation with the coarse mesh better approximates the pressure field near the injection well. At further distances away from the well XFEM and FEM give similar pressure fields. The data on this plot are at element nodes. The pressure at the well perimeter will be much higher at the edge of the well for XFEM.

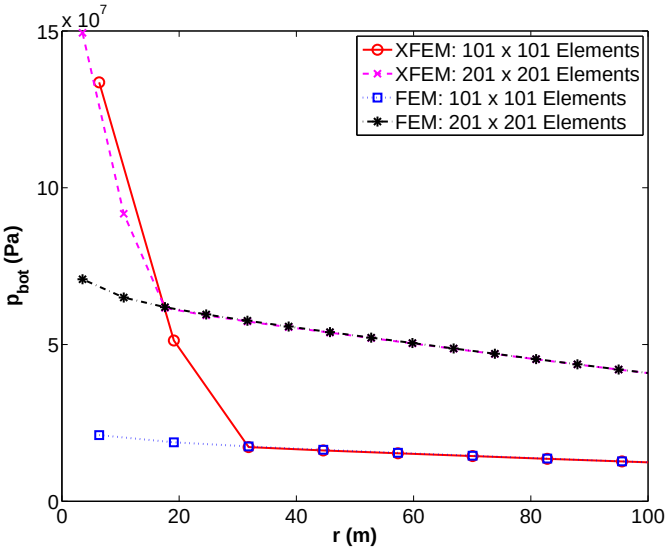

Figure 6. Comparison of XFEM and FEM pressure distributions.

Figure 7 shows the average CO_2 saturation distribution along section A-A (Figure 5). At the well the XFEM solutions give a lower CO_2 depth than does FEM. This is explained by the artificial diffusion added to stabilized the saturation equation. The amount of stabilization that is added is a function of the pressure gradient, which is significantly higher for the XFEM simulations.

A convergence study for the pressure at the well is shown in Figure 8. The pressure values are much larger here than in Figure 6 since the pressures shown in Figure 8 are taken at the edge of the well. XFEM converges rapidly towards a solution, while FEM converges much slower, and has not come close to converging for the mesh densities investigated.

The effect of the amount of non-dimensional stabilization (τ) on the average saturation profile is studied using XFEM in Figure 9. At low values of τ the saturation profile is non-physical. The approximation is improved as τ is increased. One side effect of increased damping is the reduction of the depth of CO_2 at the injection well. The amount of stabilization added is amplified for XFEM due to a larger pressure gradient (see (43)). The effect of τ on the pressure is shown in Figure 10. Once τ is large enough to eliminate the non-physical values, there is little change in the pressure field for the values of τ shown.

6.2. *Example 2*

In this example CO_2 is injected into a sloping aquifer. The problem is illustrated in Figure 11 and the system properties are described in Table II. The aquifer is bounded above and below by impermeable layers. The top boundary of the aquifer slopes upwards to the right and the bottom boundary slopes downwards to the right. Therefore, the depth of the aquifer is a function of the x and y coordinates.

Dirichlet boundary conditions are specified for the pressure equations as the hydrostatic pressure caused by the brine that exists between the top of the water table and the bottom of the aquifer. For the saturation equation dirichlet boundary conditions are specified such that at the boundaries of the

DOI: 10.1002/nme

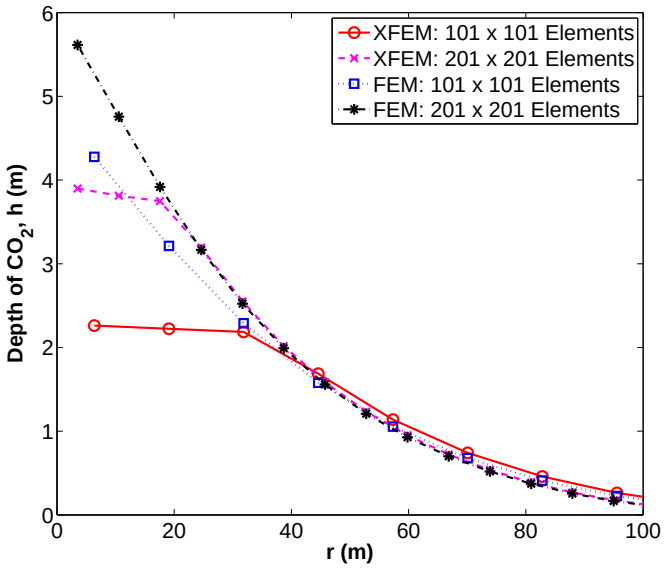

Figure 7. Comparison of XFEM and FEM average CO_2 saturation distributions.

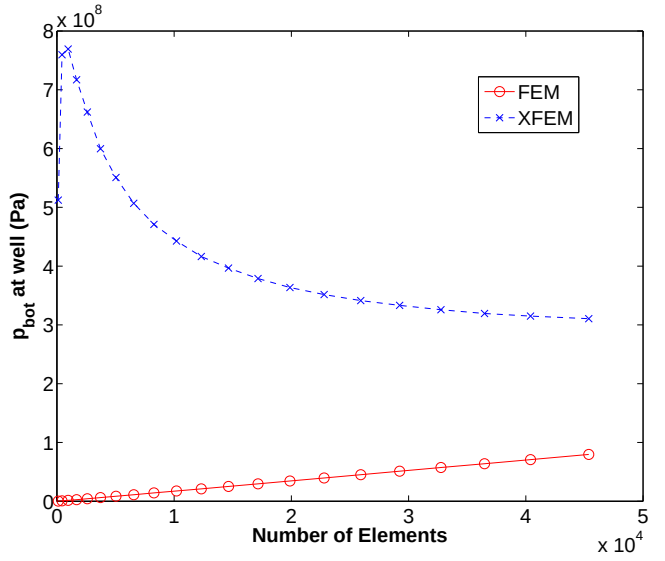

Figure 8. Comparison of convergence of pressure at the injection well for XFEM and FEM.

domain the full depth of the aquifer is filled with brine. Initial conditions of a completely brine-filled aquifer are applied.

The average CO_2 saturation profile is shown in Figure 12. Since the CO_2 has a lower density than the host brine fluid, the CO_2 should preferentially flow to the right, following the up-sloping top boundary of the aquifer.

Figure 12 shows the average saturation after 60 days of injection for the system shown in Figure 11 compared to the system shown in Figure 5. The average saturation is shown along axis b, defined in Figure 11. Comparing the evolution of the CO_2 plume in the horizontal aquifer case and the sloping aquifer we can see that the for the sloping aquifer, the CO_2 preferentially flows up the slope. This preferential flow is caused by the buoyant drive resulting from the lower density of the

DOI: 10.1002/nme

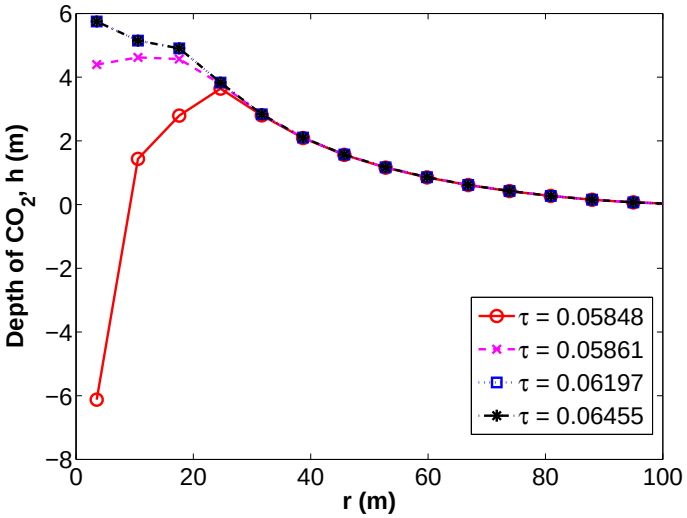

Figure 9. Effect of non-dimensional stabilization parameter on average CO_2 saturation profile.

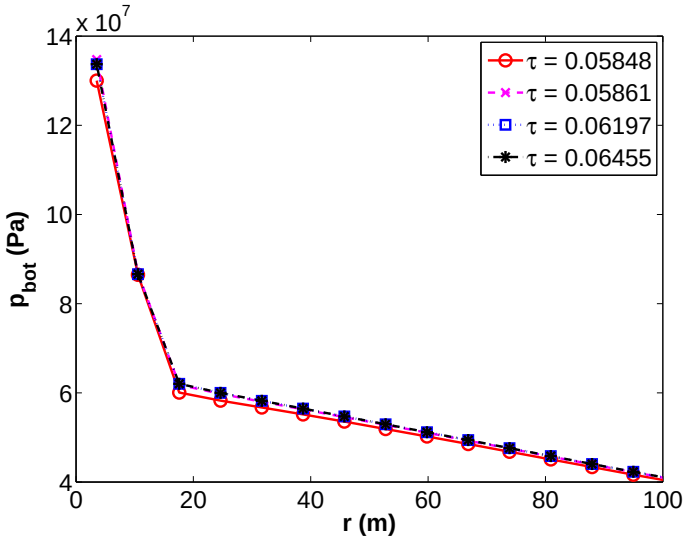

Figure 10. Effect of non-dimensional stabilization parameter on pressure.

CO_2 compared to brine. Thus the current formulation adequately captures the updip effect of CO_2 migration.

Figure 13 shows the pressure distribution along along axis b, defined in Figure 11 after 60 days of injection. The pressure field near the well is almost identical for the horizontal aquifer and the sloping aquifer, confirming that the difference in the evolution of the CO_2 is caused by the sloping aquifer and the density difference between the CO_2 and the brine. It can be concluded that during the early stages of injection the saturation of CO_2 is significantly impacted by the sloping aquifer geometry –meaning that the differences in the evolution of the CO_2 saturation field between the horizontal aquifer and the sloping aquifer are driven by buoyancy forces.

DOI: 10.1002/nme

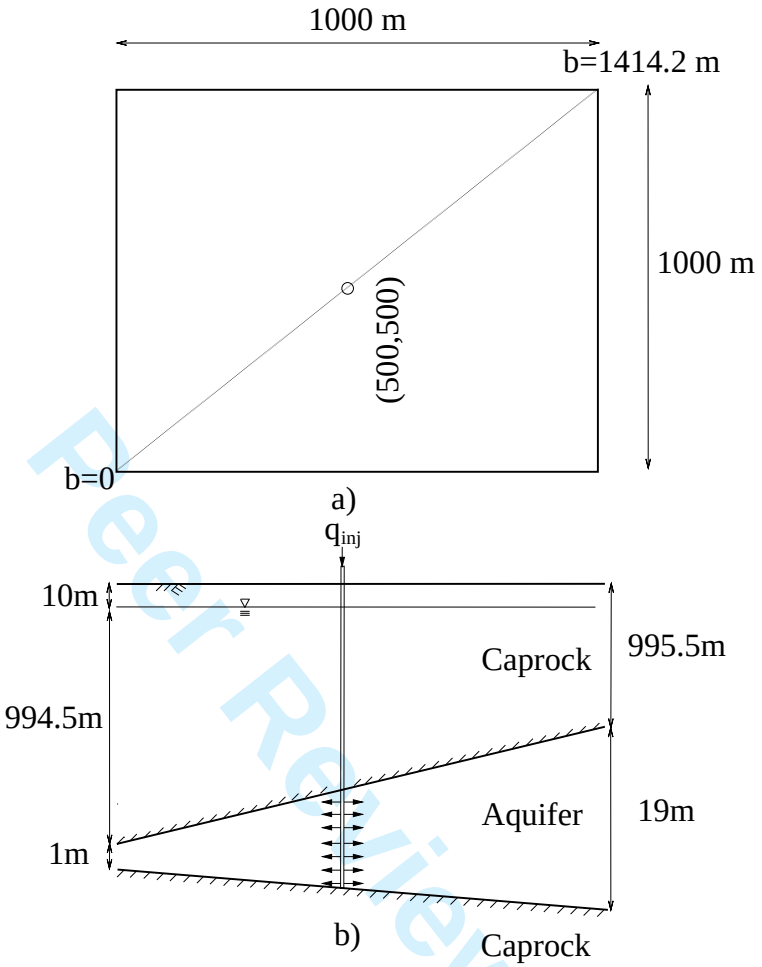

Figure 11. Set up of Example 2.

Table II. System properties for example 2.

Property	Value	Units
μ_B	5.11e-4	Ns/m^2
μ_C	6.11e-5	Ns/m^2
ρ_B	1099	kg/m^3
ρ_C	400	kg/m^3
$S_{res,B}$	0	-
ϕ	0.15	-
k_x	1e-15	m^2
k_y	1e-15	m^2
$k_{rel,C}$	1	-
q_{inj}	1600	m^3/d
r_w	0.15	m

7. CONCLUSIONS

A computationally efficient model of carbon sequestration, where carbon dioxide (CO_2) is injected into deep saline aquifers is presented. An effective computational scheme is obtained by combining the efficiency of a vertically averaged formulation and through the enrichment of the pressure

DOI: 10.1002/nme

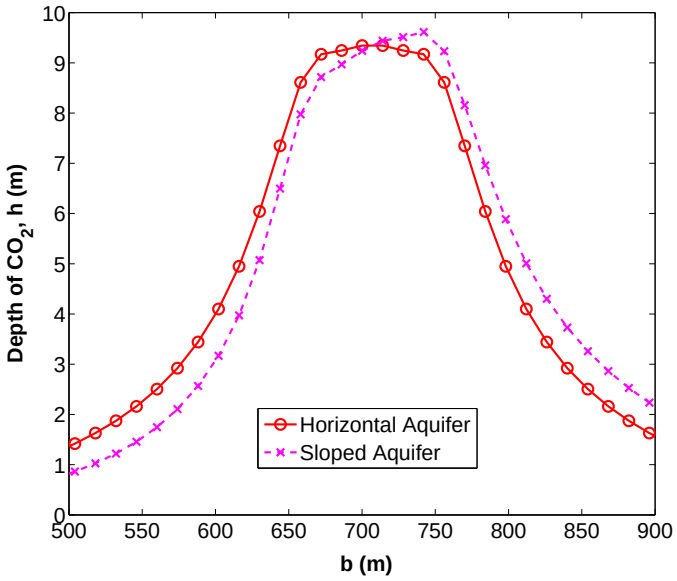

Figure 12. XFEM Average CO_2 Saturation Distribution after 60 days of injection

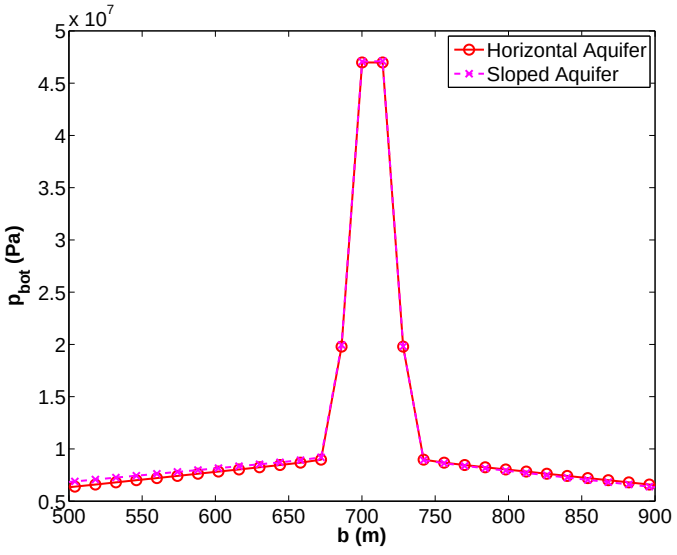

Figure 13. XFEM Pressure Distribution after 60 days of injection

approximation using the eXtended Finite Element Method (XFEM). The XFEM-based formulation is used to improve the approximation of the singular pressure field in the vicinity of an injection well. The XFEM pressure approximation is combined with a Streamline Upwind Petrov-Galerkin/ Finite Element Method/Finite Difference Method (SUPG-FEM-FDM) framework to approximates the average CO_2 saturation through the thickness of the aquifer. Using the XFEM-SUPG-FEM-FDM framework we examined two examples. In the first, it was shown that XFEM has superior convergence properties near injection wells, when compared to a FEM approximation. The pressure approximation is shown to be relatively insensitive to increases in the SUPG stabilization parameter, once stable behaviour is obtained. In the second example, the XFEM-SUPG-FEM-FD simulator is

DOI: 10.1002/nme

demonstrated to be able to capture the important effect of buoyancy driven flow of CO_2 in a sloping aquifer.

8. ACKNOWLEDGMENTS

This article is dedicated to Professor Ted Belytschko for his contributions to the field of computational mechanics, his stewardship over this field and this journal, and his mentorship of young researchers such as myself-Robert Gracie.

The authors would like to acknowledge funding from the Natural Sciences and Engineering Research Council (NSERC) and NSERC-Network of Centres of Excellence- Carbon Management Canada and the Ontario Graduate Scholarship (OGS).

REFERENCES

1. R. Gracie and J. Craig, "Modelling well leakage in multilayer aquifer systems using the extended finite element method," *Finite Elements in Analysis and Design*, vol. 46, no. 6, pp. 504–513, 2010.
2. J. Craig and R. Gracie, "Using the extended finite element method for simulation of transient well leakage in multilayer aquifers," *Advances in Water Resources*, 2011.
3. T. Belytschko, R. Gracie, and G. Ventura, "A review of extended/generalized finite element methods for material modeling," *Modelling and Simulation in Materials Science and Engineering*, vol. 17, no. 4, p. 043001, 2009.
4. T.-P. Fries and T. Belytschko, "The extended/generalized finite element method: an overview of the method and its applications," *International Journal for Numerical Methods in Engineering*, vol. 84, no. 3, pp. 253–304, 2010.
5. S. Pommier, A. Gravouil, N. Moes, and A. Combescure, *Extended finite element method for crack propagation*. Wiley. com, 2013.
6. S. Mohammadi, *XFEM Fracture Analysis of Composites*. Wiley. com, 2012.
7. N. Moës, J. Dolbow, and T. Belytschko, "A finite element method for crack growth without remeshing," *International Journal for Numerical Methods in Engineering*, vol. 46, pp. 131–150, 1999.
8. J. Dolbow, N. Moës, and T. Belytschko, "Modeling fracture in mindlin–reissner plates with the extended finite element method," *International Journal of Solids and Structures*, vol. 37, no. 48, pp. 7161–7183, 2000.
9. Z. Liu, T. Menouillard, and T. Belytschko, "An xfem/spectral element method for dynamic crack propagation," *International Journal of Fracture*, vol. 169, no. 2, pp. 183–198, 2011.
10. T. Menouillard and T. Belytschko, "Smoothed nodal forces for improved dynamic crack propagation modeling in xfem," *International Journal for Numerical Methods in Engineering*, vol. 84, no. 1, pp. 47–72, 2010.
11. H. Nguyen-Vinh, I. Bakar, M. Msekh, J.-H. Song, J. Muthu, G. Zi, P. Le, S. Bordas, R. Simpson, S. Natarajan, *et al.*, "Extended finite element method for dynamic fracture of piezo-electric materials," *Engineering Fracture Mechanics*, vol. 92, pp. 19–31, 2012.
12. M. Holl, S. Loehnert, and P. Wriggers, "An adaptive multiscale method for crack propagation and crack coalescence," *International Journal for Numerical Methods in Engineering*, vol. 93, no. 1, pp. 23–51, 2013.
13. P. Aubertin, J. Rethore, and R. de Borst, "Dynamic crack propagation using a combined molecular dynamics/extended finite element approach," *International Journal for Multiscale Computational Engineering*, vol. 8, no. 2, 2010.
14. R. Gracie and T. Belytschko, "An adaptive concurrent multiscale method for the dynamic simulation of dislocations," *International Journal for Numerical Methods in Engineering*, vol. 86, no. 4-5, pp. 575–597, 2011.
15. J. Oswald, E. Wintersberger, G. Bauer, and T. Belytschko, "A higher-order extended finite element method for dislocation energetics in strained layers and epitaxial islands," *International journal for numerical methods in engineering*, vol. 85, no. 7, pp. 920–938, 2011.
16. X. Liu, H. Waisman, and J. Fish, "A new crack tip enrichment function in the extended finite element method for general inelastic materials," *International Journal for Multiscale Computational Engineering*, vol. 10, no. 4, 2012.
17. O. Skiba, R. Gracie, and S. Potapenko, "Electromechanical simulations of dislocations," *Modelling and Simulation in Materials Science and Engineering*, vol. 21, no. 3, p. 035003, 2013.
18. J. Chessa and T. Belytschko, "An extended finite element method for two-phase fluids," *Journal OF Applied Mechancis-Transactions of the ASME*, vol. 70, no. 1, pp. 10–17, 2003.
19. K.-W. Cheng and T.-P. Fries, "Xfem with hanging nodes for two-phase incompressible flow," *Computer Methods in Applied Mechanics and Engineering*, 2012.
20. H. Sauerland and T.-P. Fries, "The stable xfem for two-phase flows," *Computers & Fluids*, 2012.
21. T. Mohammadnejad and A. Khoei, "An extended finite element method for fluid flow in partially saturated porous media with weak discontinuities; the convergence analysis of local enrichment strategies," *Computational Mechanics*, vol. 51, no. 3, pp. 327–345, 2013.
22. M. A. Celia and J. M. Nordbotten, "Practical modeling approaches for geological storage of carbon dioxide," *Ground Water*, vol. 47, no. 5, pp. 627–638, 2009.
23. J. Nordbotten and M. Celia, "Analysis of plume extent using analytical solutions for co_2 storage," in *Proceedings of the 16th conference on Computational Methods in Water Resources*, 2006.
24. J. Nordbotten and M. Celia, "Similarity solutions for fluid injection into confined aquifers," *Journal of Fluid Mechanics*, vol. 561, pp. 307–327, 2006.

25. J. Nordbotten, M. Celia, S. Bachu, and H. Dahle, "Semianalytical solution for co_2 leakage through an abandoned well," *Environmental science & technology*, vol. 39, no. 2, pp. 602–611, 2005.
26. J. Nordbotten, M. Celia, D. Kavetski, and S. Bachu, "A semi-analytical model estimating leakage associated with co_2 storage in large-scale multi-layered geological systems with multiple leaky wells," *Environmental Science and Technology*, vol. 43, no. 3, pp. 743–749, 2009.
27. T.-P. Fries, "A corrected xfem approximation without problems in blending elements," *International Journal for Numerical Methods in Engineering*, vol. 75, no. 5, pp. 503–532, 2008.
28. A. N. Brooks and T. J. Hughes, "Streamline upwind/petrov-galerkin formulations for convection dominated flows with particular emphasis on the incompressible navier-stokes equations," *Computer methods in applied mechanics and engineering*, vol. 32, no. 1, pp. 199–259, 1982.
29. H. Stone and A. Garder Jr, "Analysis of gas-cap or dissolved-gas drive reservoirs," *SPE Journal*, vol. 1, no. 2, pp. 92–104, 1961.